

ENVIRONMENTAL RESEARCH
LETTERS

LETTER

OPEN ACCESS

RECEIVED
15 July 2021REVISED
28 August 2021ACCEPTED FOR PUBLICATION
15 September 2021PUBLISHED
29 September 2021

Original Content from
this work may be used
under the terms of the
[Creative Commons
Attribution 4.0 licence](#).

Any further distribution
of this work must
maintain attribution to
the author(s) and the title
of the work, journal
citation and DOI.

Combining CMIP data with a regional convection-permitting model
and observations to project extreme rainfall under climate change

Cornelia Klein^{1,7,*} , Lawrence S Jackson² , Douglas J Parker² , John H Marsham²,
Christopher M Taylor^{1,8} , David P Rowell³, Françoise Guichard^{4,11}, Théo Vischel⁵, Adjoua Moïse Famien^{6,9}
and Arona Diedhiou^{5,10}

- ¹ U.K. Centre for Ecology and Hydrology, Wallingford, United Kingdom
 - ² Institute for Climate and Atmospheric Science, University of Leeds, Leeds, United Kingdom
 - ³ Met Office Hadley Centre, Exeter, United Kingdom
 - ⁴ CNRM, Université de Toulouse, Météo-France, CNRS, Toulouse, France
 - ⁵ Université Grenoble Alpes, IRD, CNRS, Grenoble-INP, IGE, Grenoble, France
 - ⁶ LOCEAN, Sorbonne Universités UPMC-CNRS-IRD-MNHN, IPSL, Paris, France
 - ⁷ Department of Atmospheric and Cryospheric Sciences, University of Innsbruck, Innsbruck, Austria
 - ⁸ National Centre for Earth Observation, Wallingford, United Kingdom
 - ⁹ Université Félix Houphouët Boigny, LAPAMF-UFR SSMT, Abidjan, Côte d'Ivoire
 - ¹⁰ Centre d'Excellence Africain en Changement Climatique, Biodiversité et Agriculture Durable (CCBAD), Université Félix Houphouët Boigny, Abidjan, Côte d'Ivoire
 - ¹¹ Deceased December 2020
- * Author to whom any correspondence should be addressed.

E-mail: cornkle@ceh.ac.uk

Keywords: CMIP, mesoscale convective system, West Africa, climate projection, atmospheric moisture scaling, convection-permitting, extreme rainfall

Supplementary material for this article is available [online](#)

Abstract

Due to associated hydrological risks, there is an urgent need to provide plausible quantified changes in future extreme rainfall rates. Convection-permitting (CP) climate simulations represent a major advance in capturing extreme rainfall and its sensitivities to atmospheric changes under global warming. However, they are computationally costly, limiting uncertainty evaluation in ensembles and covered time periods. This is in contrast to the Climate Model Intercomparison Project (CMIP) 5 and 6 ensembles, which cannot capture relevant convective processes, but provide a range of plausible projections for atmospheric drivers of rainfall change. Here, we quantify the sensitivity of extreme rainfall within West African storms to changes in atmospheric rainfall drivers, using both observations and a CP projection representing a decade under the Representative Concentration Pathway 8.5 around 2100. We illustrate how these physical relationships can then be used to reconstruct better-informed extreme rainfall changes from CMIP, including for time periods not covered by the CP model. We find reconstructed hourly extreme rainfall over the Sahel increases across all CMIP models, with a plausible range of 37%–75% for 2070–2100 (mean 55%, and 18%–30% for 2030–2060). This is considerably higher than the +0–60% (mean +30%) we obtain from a traditional extreme rainfall metric based on raw daily CMIP rainfall, suggesting such analyses can underestimate extreme rainfall intensification. We conclude that process-based rainfall scaling is a useful approach for creating time-evolving rainfall projections in line with CP model behaviour, reconstructing important information for medium-term decision making. This approach also better enables the communication of uncertainties in extreme rainfall projections that reflect our current state of knowledge on its response to global warming, away from the limitations of coarse-scale climate models alone.

1. Introduction

Convective rainfall dominates rainfall extremes in many regions of the world, which are set to increase with or beyond the rate of increasing water vapour in the atmosphere in a warming climate (Allen and Ingram 2002, O’Gorman and Schneider 2009). Vigorous convective events can pose a serious threat to human health, urban infrastructure, and food security by causing flash floods (Lobell and Gourdjji 2012, Engel *et al* 2017). Yet, projected changes in extreme rainfall remain highly uncertain (IPCC 2021). This is in part because traditional coarse-scale global climate models with horizontal resolutions commonly ≥ 100 km, such as those in the Climate Model Intercomparison Project (CMIP) ensembles, cannot explicitly capture convective processes. Instead, these models rely on convective parameterisations that tend to produce daily rainfall intensities that are too low and spread out, rendering projected changes in extreme precipitation questionable (Trenberth *et al* 2003, Stephens *et al* 2010). This severely limits the usefulness of climate projections in the context of local impacts of changes in extreme weather (e.g. Vischel *et al* 2007). Consequently, there is an urgent need for more reliable information on future trends in rainfall extremes, which can support the development of adaptation and mitigation strategies.

In this context, convection-permitting (CP) simulations, which allow convection to develop explicitly, have been found to simulate more realistic rainfall characteristics in different convective environments (Prein *et al* 2015, Kendon *et al* 2017). However, such simulations are computationally expensive and therefore often conducted in a one-off manner, providing a single realisation of a possible future without capturing uncertainties intrinsic to future climate projections. Ensemble projections at CP scale are only just starting to emerge e.g. with a focus on the UK (Fosser *et al* 2020), or are still under planning e.g. within Coordinated Regional Climate Downscaling Experiment (CORDEX) Flagship Pilot Studies for Europe, South America, and High Mountain Asia (Coppola *et al* 2020, Lavin-Gullon *et al* 2021, Zhou *et al* 2021).

Currently, the best way to evaluate future rainfall extremes and related risks must be an expert-informed approach that combines the advantages of information from existing parameterised and CP climate model projections, together with understanding from observations. This study brings together these different state-of-the-art climate data to derive future extreme rainfall estimates.

We focus on West Africa, where we now have a single CP realisation of future climate (Stratton *et al* 2018, Senior *et al* 2021), which shows a greater increase in extreme rainfall than a parameterised version of the model, with greater intensification of

convective updraughts (Berthou *et al* 2019, Kendon *et al* 2019, Fitzpatrick *et al* 2020, Jackson *et al* 2020). This CP simulation is a major advance given the dominance of large, organised thunderstorm-clusters in this region, which produce the majority of extreme rainfall (Mathon *et al* 2002). These so-called meso-scale convective systems (MCSs) however cannot be captured by CMIP models. We demonstrate an approach for combining the individual CP projection with rainfall-driver relationships from observations and with the uncertainty range from 64 CMIP simulations, based on their future changes in atmospheric MCS drivers.

Variability and change in extreme MCS rainfall predominantly depends on total column water (TCW), low-level vertical wind shear and convective available potential energy (CAPE). Higher TCW content in a warmer atmosphere is known to intensify storm dynamics and to strongly control increases in extreme rainfall (Roderick *et al* 2019, Fitzpatrick *et al* 2020, Lenderink *et al* 2021). Wind shear affects MCS organisation (Moseley *et al* 2016), the entrainment dilution of convection (Mulholland *et al* 2021) and the inflow of unstable air and hence latent heating (Alfaro 2017), thereby modifying MCS intensity (Mohr and Thorncroft 2006). Environmental CAPE is another important driver for changes in MCS intensities and size (Prein *et al* 2017, Maranan *et al* 2018), but strongly co-varies with TCW and is therefore excluded from the driver scaling here to avoid double-counting. We therefore focus on future TCW and wind shear changes in CMIP models to reconstruct probable and time-continuous extreme MCS rainfall intensities.

Future changes in extreme rainfall and associated uncertainty are key parameters for defining long-term adaptation strategies against hydrological risks. The design of hydraulic infrastructures (e.g. sewage systems, dams) and their management relies on statistical indicators such as intensity-duration-frequency curves, design rainfall or floods, whose estimation in a changing climate remains a major challenge (Francois *et al* 2019, Brunner *et al* 2021, Sharma *et al* 2021). This is particularly the case in West Africa, where hydraulic design tools are non-existent or obsolete (Sane *et al* 2018). We illustrate a way to use CP models in combination with observations to inform the use of coarse-scale climate model data for such estimations. To our knowledge, this is the first attempt to combine this mixture of models and observations to better understand the response of future rainfall extremes to its atmospheric drivers.

2. Datasets and method

2.1. Observation-based data

Following the methodology in Klein *et al* (2021), and drawing on previous West African studies (Arnaud *et al* 1992, Laing *et al* 1999, Mathon *et al* 2002),

we use thermal-infrared imagery from the Meteosat series, which we combine with microwave rainfall estimates, and ERA5 reanalysis data over the West African monsoon season May–October 2004–2018 to relate MCS rainfall intensities to atmospheric drivers. Together, these datasets capture a broad range of MCS-driver variability under current climate conditions.

Based on 10.8 μm -band brightness temperatures of the Meteosat Second Generation (MSG; Schmetz *et al* 2002, EUMETSAT 2021), we identify MCSs as contiguous cloud $\leq -50^\circ\text{C}$ regions larger than 5000 km^2 between 16 and 1900UTC, the time when the frequency of MCSs reaches a maximum (e.g. Mathon and Laurent 2001), for a Sahelian domain (9° – 19° N, 10° W– 15° E). Maximum MCS rainfall (P_{max}) is sampled from matched-up ‘high-quality precipitation’ (HQprecipitation, merged microwave-only precipitation estimate) fields of the half-hourly Final Run V06B Integrated Multi-satellite Retrievals for Global Precipitation Measurement (IMERG-HQ; Huffman *et al* 2019) dataset at ~ 15 km resolution. MCS snapshots with $P_{\text{max}} \leq 1 \text{ mm h}^{-1}$ are removed to exclude non-precipitating cloud shields. We thus obtain conditional maximum rain rates from 22 368 MCS snapshots, for which we identify pre-storm driver conditions.

Environmental TCW and wind shear, defined here as the 925–600 hPa zonal wind difference in m s^{-1} , are sampled from ERA5 reanalysis hourly data (Hersbach *et al* 2020, CDS 2021) coarsened to 0.7° resolution at 1200UTC, preceding afternoon MCSs, and at the location of minimum MCS temperature. The 0.7° resolution for atmospheric drivers reflects the scale of smallest considered MCSs while ensuring better consistency with the coarse spatial resolution of CMIP model data. For brevity, we refer to the combination of MSG, IMERG-HQ and ERA5 data for analyses as observation-based (OBS).

2.2. Convection-permitting model

This study uses data from the CP4 simulation; a 4.4 km pan-African CP climate simulation based on the Met Office Unified Model and created within the Future Climate for Africa (FCFA) Improving Model Processes for African cLimAte (IMPALA) project (Stratton *et al* 2018, Kendon *et al* 2019). The modelled historical period (CP4_H) encompasses 1997–2006 with atmospheric boundary conditions provided by a prototype of the latest atmosphere-only UM global model GA7/GL7 at 25 km with sea-surface temperatures (SST) prescribed from observations (Reynolds *et al* 2007). The CP4 future projection (CP4_F) covers ten years representative of 2100 climate conditions. It uses GA7/GL7 atmospheric boundary conditions under increased greenhouse gas concentrations in line with the Representative Concentration pathway (RCP) 8.5 at the end of this century. Driving SSTs are

adjusted from CP4_H to reflect end-of-century SSTs by adding a climatological annual cycle of ΔT derived from a HadGEM2-ES climate projection (Jones *et al* 2011), while ozone and aerosol concentrations in CP4_F remain the same as for CP4_H.

At ~ 4.4 km resolution, CP4 operates within the ‘grey zone’ for resolving convection (Field *et al* 2017), but has been confirmed to improve the intensity and distribution of precipitation across the Sahel (Berthou *et al* 2019). It also correctly captures climatological MCS distributions, albeit with underestimations in maximum MCS size and speeds together with an overestimation in MCS frequencies (Crook *et al* 2019). We extract simulated afternoon MCSs following the same approach as for OBS, converting outgoing longwave radiation into brightness temperatures and applying the $\leq -50^\circ\text{C}$ temperature threshold. Filtering for $\geq 5000 \text{ km}^2$ rainy clouds gives 45 977 MCS snapshots for CP4_H and 35 975 snapshots for CP4_F with co-located atmospheric conditions sampled at 1200UTC and at 0.7° resolution. The smaller number of future MCSs is consistent with previous CP4 analyses, which found fewer but more intense rain events paired with longer dry spells across the Sahel for CP4_F (Berthou *et al* 2019, Kendon *et al* 2019). In line with IMERG-HQ rainfall, the modelled rainfall is coarsened to 15 km resolution before sampling MCS maximum rainfall. This averaging also reduces the overestimation of high-intensity rainfall CP4 shows at native resolution (cf supplementary figure S1, Berthou *et al* 2019).

2.3. CMIP models

We analyse driver changes in wind shear and TCW out to 2100 in simulations from 38 CMIP5 (Taylor *et al* 2012) and 26 CMIP6 models (Eyring *et al* 2016); one realisation per model i.e. ‘r1i1p1’ members (see supplementary table 1; available online at stacks.iop.org/ERL/16/104023/mmedia) for which data were available for both variables. Only simulations forced by the RCP 8.5 (Shared Socioeconomic Pathway 5-8.5 for CMIP6) are analysed, consistent with CP4. Three different 30-year time slices are considered; 2030–2059 (‘2040’), 2050–2079 (‘2060’), and 2070–2099 (‘2080’). The reference period covers 1950–1999, which was driven by historical anthropogenic and natural forcings. The models were interpolated onto a common 1.25° latitude \times 1.875° longitude grid and averaged for respective time slices. For the rainfall reconstruction, we use a seasonal average of the changes in atmospheric drivers during the peak monsoon months July–September (JAS), during which MCS activity is at a maximum in the Sahel (Lafare *et al* 2011, Nicholson 2018). For a subset of models, we also evaluate changes in 3-hourly and daily rainfall extremes, depending on availability (cf supplementary table 1).

2.4. Translating driver changes into changes in extreme rainfall

Using the identified MCSs from OBS and CP4, we define MCS extreme rainfall as the 95th percentile of the maximum MCS rainfall distribution ($P_{\max^{95}}$). We assume a linear relationship between changes in $\Delta P_{\max^{95}}$ and atmospheric driver changes. The individual driver contribution is then defined as

$$\Delta P_{\max^{95},t} = \beta_t \times \Delta \text{TCW}, \quad (1)$$

and

$$\Delta P_{\max^{95},s} = \beta_s \times \Delta \text{shear}, \quad (2)$$

where ΔTCW and Δshear denote the differences between JAS average future and historical conditions of the respective variable from either CMIP models or CP4. Reconstructed rainfall from JAS CP4-drivers will be used to evaluate our scaling approach in comparison to the CP4 modelled rainfall change. β_t and β_s represent the associated rainfall/driver relationships based on hourly atmospheric data, either as simulated by CP4 or derived from OBS. The change in driver-based $P_{\max^{95}}$ is then reconstructed as a linear combination of individual driver contributions:

$$\Delta P_{\max^{95},t+s} = \Delta P_{\max^{95},t} + \Delta P_{\max^{95},s}. \quad (3)$$

Our use of the driver scaling factors β_t and β_s depends on the precipitation/driver relationship remaining the same in the current and future climates, and on CP4 capturing the relationship under both climates. This will be discussed in the following.

3. Derived rainfall-driver relationships

3.1. Historical scaling of observed and modelled extreme rainfall with atmospheric drivers

We first evaluate how the rainfall-driver scaling compares between OBS and CP4_H for the atmospheric drivers TCW and shear. In figures 1(a) and (b), we stratify the MCS sample according to driver strength and compute the 95th percentile of the P_{\max} distribution to obtain the intensity of the 5% most intense storms that can be supported by any joint TCW-shear combination (i.e. $P_{\max^{95}}$). This allows us to ascertain how $P_{\max^{95}}$ changes in response to one driver while the other remains approximately constant.

There is a marked tendency for $P_{\max^{95}}$ to increase with higher TCW as well as with wind shear in OBS (figure 1(a)). This behaviour cannot be explained by any correlation between TCW and shear, which is negative for OBS ($r = -0.21$, $p \leq 0.01$). CP4_H similarly shows higher $P_{\max^{95}}$ as TCW increases, but exhibits little sensitivity to ambient shear. Averaging across TCW-bins, figure 1(c) confirms that CP4_H $P_{\max^{95}}$ -scaling with TCW shows good correspondence with a rainfall change of 0.69 mm h^{-1} per unit increase in TCW (mm) compared to 0.71 mm h^{-1} for OBS. At

the same time, CP4_H considerably underestimates the rainfall spread introduced by wind shear per TCW-bin (blue spread) and consequently does not reproduce the observed $P_{\max^{95}}$ -increase of 0.78 mm h^{-1} per unit shear (m s^{-1}) shown in figure 1(d).

This result is in line with previous studies of CP4, which found realistic MCS rainfall sensitivity to TCW but little shear dependency (Fitzpatrick *et al* 2020, Senior *et al* 2021). Our observation-based results however highlight the importance of shear for MCS maximum rainfall intensity on synoptic time scales; a relationship which is backed by theory (Alfaro 2017) and can be captured by idealised models below 1 km spatial resolution (Bickle *et al* 2021).

We will therefore rely on the historical absolute $P_{\max^{95}}$ -shear scaling as inferred from OBS following equation (2) with β_s defined as

$$\beta_s = \left(\frac{\partial P_{\max^{95}}}{\partial \text{shear}} \right)_{\text{OBS}} = 0.78 \pm 0.15 \frac{\text{mm h}^{-1}}{\text{m s}^{-1}} \quad (\pm \text{SE}) \quad (4)$$

representing the absolute change in rainfall per unit shear from observations (figure 1(d)) \pm standard error (SE). This is applied under the assumption that scaling of rainfall with wind shear remains constant across climates, which is supported by the good fit of the layer-lifting model of convection in Bickle *et al* (2021), since this model depends on MCS-relative flows of moisture and hence shear. For TCW on the other hand, CP4 shows realistic behaviour, which we exploit in the next step to derive the scaling of $P_{\max^{95}}$ with increasing TCW under global warming.

3.2. Future scaling of extreme rainfall with atmospheric moisture

Based on end-of-century projected changes by CP4, we now consider the climate change sensitivity of $P_{\max^{95}}$ to TCW relative to the historical period. Different from the effect of wind shear, the rainfall-humidity relationship cannot be assumed to remain the same across climates as similar levels of TCW do not result in similar rainfall intensities.

This is illustrated in figure 2, where in addition to CP4_H, the pre-storm atmospheric drivers are separated for CP4_F MCSs, similar to the approach used to obtain figure 1(c), but by averaging the $P_{\max^{95}}$ distribution across 5-percentile TCW-bins. Compared to CP4_H, the CP4_F MCS distribution shows a marked shift towards higher TCW. At the same time, when MCSs occur, similar levels of TCW in CP4_F result in higher $P_{\max^{95}}$ than in CP4_H. This is in contrast to our current understanding for likely changes in mean rainfall, for which less rainfall is expected in a warmer climate for similar TCW, as more moisture is necessary to reach similar levels of relative humidity. A possible explanation for this behaviour is that extreme MCS rainfall occurs when convection is strong. Convective updraughts are expected to widen

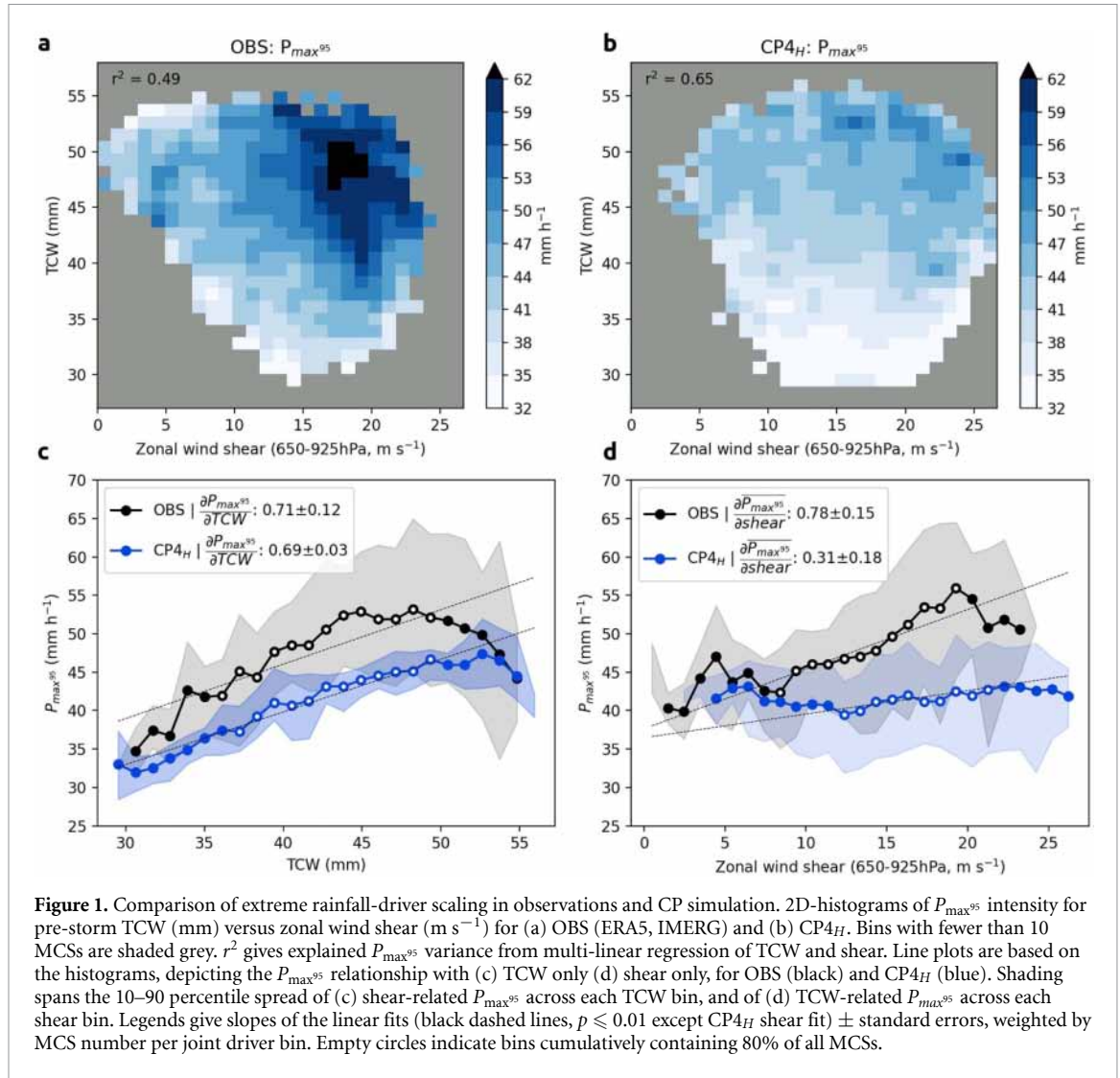


Figure 1. Comparison of extreme rainfall-driver scaling in observations and CP simulation. 2D-histograms of P_{\max}^{95} intensity for pre-storm TCW (mm) versus zonal wind shear (m s^{-1}) for (a) OBS (ERA5, IMERG) and (b) CP4_H. Bins with fewer than 10 MCSs are shaded grey. r^2 gives explained P_{\max}^{95} variance from multi-linear regression of TCW and shear. Line plots are based on the histograms, depicting the P_{\max}^{95} relationship with (c) TCW only (d) shear only, for OBS (black) and CP4_H (blue). Shading spans the 10–90 percentile spread of (c) shear-related P_{\max}^{95} across each TCW bin, and of (d) TCW-related P_{\max}^{95} across each shear bin. Legends give slopes of the linear fits (black dashed lines, $p \leq 0.01$ except CP4_H shear fit) \pm standard errors, weighted by MCS number per joint driver bin. Empty circles indicate bins cumulatively containing 80% of all MCSs.

and intensify under global warming (Prein et al 2017), with the latter similarly identified for CP4 (Jackson et al 2020). The dynamical MCS intensification may then result in higher extreme rainfall in the future for similar TCW levels.

We follow a ‘quantile-projection’ approach to map the historical driver distribution and associated P_{\max}^{95} onto future conditions, as represented by climate change vectors β_t between CP4_F and CP4_H in figure 2. The resulting β_t ranges from 1.07 up to 1.33 (figure 2(a) inset), with a mean β_t according to

$$\beta_t = \left(\frac{\Delta P_{\max}^{95}}{\Delta \text{TCW}} \right)_{\text{CP4}} = 1.2 \pm 0.13 \text{ h}^{-1} (\pm \text{min}/\text{max}). \quad (5)$$

The fact that hourly extreme rain scales with preceding TCW with $\beta_t > 1$ points towards the importance of dynamical processes that help to increase the vertical transport of moisture in MCSs and the MCS moisture supply from the surroundings. In the following, β_t is used to calculate $P_{\max}^{95,t}$ from TCW changes in CMIP models.

4. Combined driver-based projected changes in extreme rain

We now derive a plausible range of changes in reconstructed ΔP_{\max}^{95} based on the Sahel domain-average of absolute changes in TCW (mm, figure 3(a)) and wind shear (m s^{-1} , figure 3(b)) of 64 CMIP models. The domain average is calculated for 9°–19° N, 10° W–15° E, in line with the domain where MCSs were sampled.

In terms of TCW and shear projections, there is no indication of a fundamentally different behaviour between CMIP5 and CMIP6 ensembles (figures 3(a) and (b)), justifying our pooled evaluation. For the 2080 period, the 10–90 percentile spread in TCW across all 64 CMIP models reaches +11–21 mm while CP4 projects a larger TCW change than 90% of all CMIP models (22 mm), noting it is representative of a later period and excludes anomalous aerosol forcing. Similarly, the CP4 wind shear change of +3 m s^{-1} is at the high end of the CMIP distribution.

Based on these results for ΔTCW and Δshear , we calculate $\Delta P_{\max}^{95,t}$, the rainfall contribution from

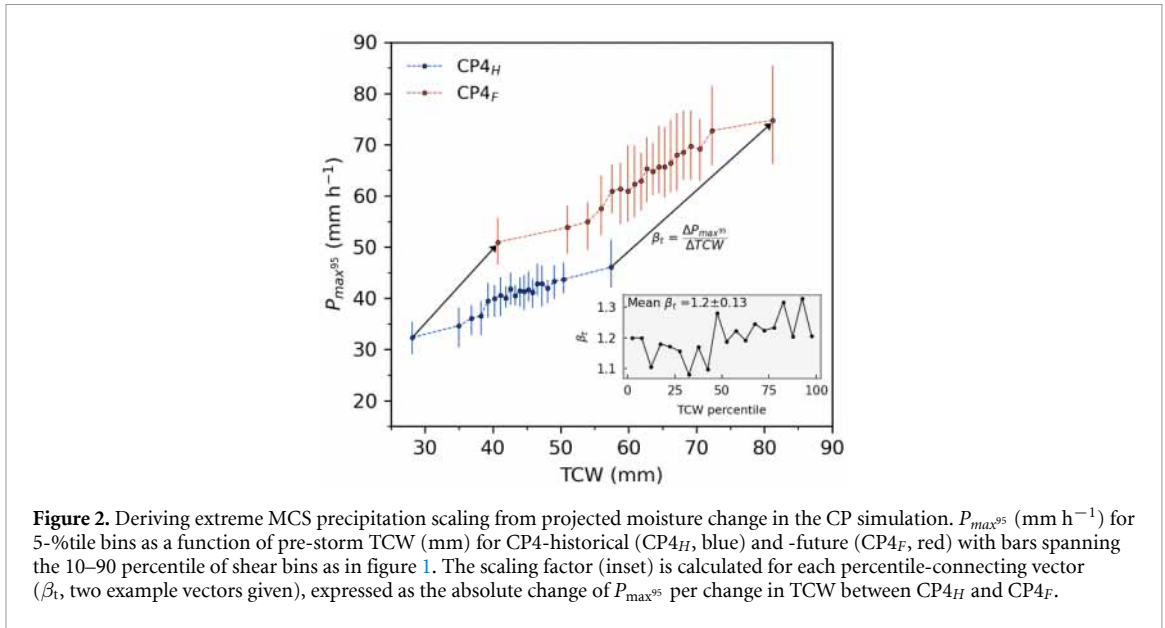


Figure 2. Deriving extreme MCS precipitation scaling from projected moisture change in the CP simulation. P_{max}^{95} (mm h^{-1}) for 5-%tile bins as a function of pre-storm TCW (mm) for CP4-historical (CP4_H, blue) and -future (CP4_F, red) with bars spanning the 10–90 percentile of shear bins as in figure 1. The scaling factor (inset) is calculated for each percentile-connecting vector (β_t , two example vectors given), expressed as the absolute change of P_{max}^{95} per change in TCW between CP4_H and CP4_F.

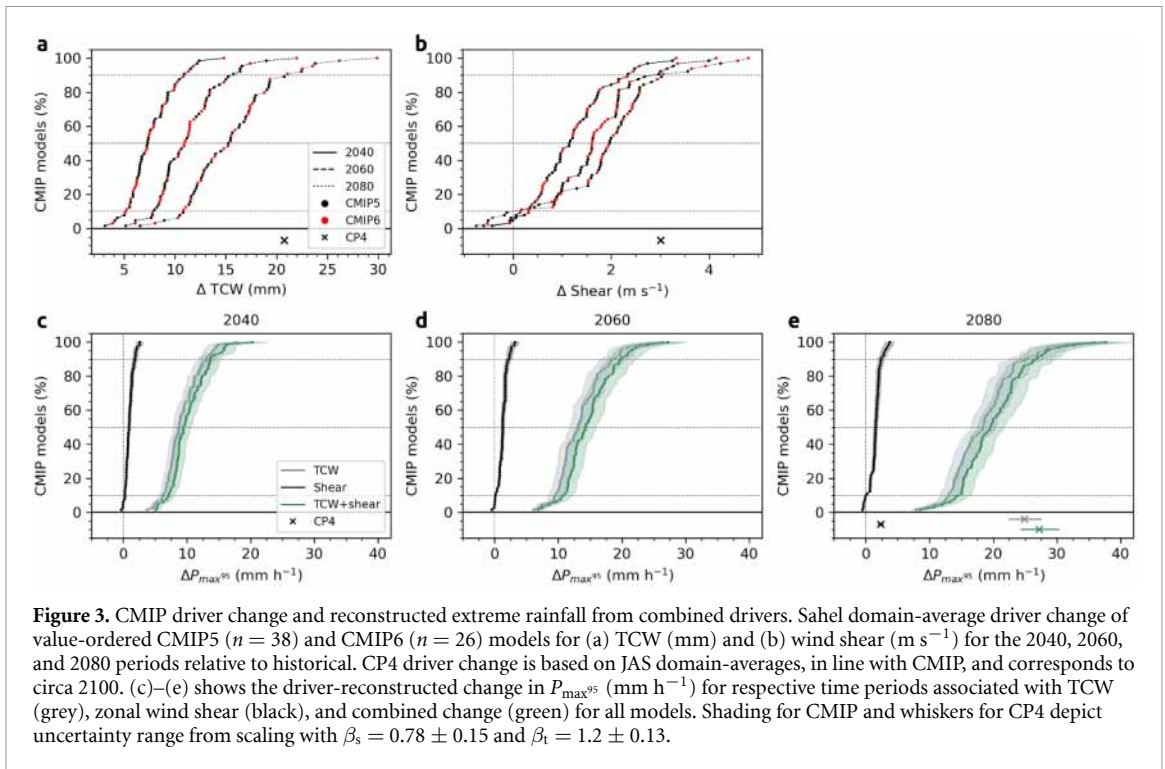


Figure 3. CMIP driver change and reconstructed extreme rainfall from combined drivers. Sahel domain-average driver change of value-ordered CMIP5 ($n = 38$) and CMIP6 ($n = 26$) models for (a) TCW (mm) and (b) wind shear (m s^{-1}) for the 2040, 2060, and 2080 periods relative to historical. CP4 driver change is based on JAS domain-averages, in line with CMIP, and corresponds to circa 2100. (c)–(e) shows the driver-reconstructed change in P_{max}^{95} (mm h^{-1}) for respective time periods associated with TCW (grey), zonal wind shear (black), and combined change (green) for all models. Shading for CMIP and whiskers for CP4 depict uncertainty range from scaling with $\beta_s = 0.78 \pm 0.15$ and $\beta_t = 1.2 \pm 0.13$.

TCW, via equation (1) using β_t as derived from CP4 (equation (5)). The scaling factor β_s from OBS (equation (4)) is directly applied in equation (2) to derive $\Delta P_{max}^{95,s}$, the rainfall contribution from shear. By scaling the CMIP driver changes throughout the century, we can also obtain reconstructed P_{max}^{95} intensities for the 2040 and 2060 periods, which are not covered by the CP4 simulation.

Using the combined information from OBS, CP4 and CMIP models, figures 3(c)–(e) finally illustrates the translation of the MCS driver changes into absolute change in reconstructed P_{max}^{95} for individual and combined drivers (c.f. equation (3)) across the different future 30-year time slices:

$$\Delta P_{max}^{95,t+s} = (\beta_t)_{CP4} \times (\Delta TCW)_{CMIP} + (\beta_s)_{OBS} \times (\Delta shear)_{CMIP} \quad (6)$$

Comparing TCW-reconstructed (figures 3(c)–(e), grey line and shading) to the combined-driver ΔP_{max}^{95} (green line and shading), we find that shear changes have a minor effect on future rainfall change: while the individual change related to shear still increases from $+1.8 \text{ mm h}^{-1}$ around 2040 to $+2.4 \text{ mm h}^{-1}$ by 2080 for the 90th CMIP percentile, the relative contribution from strengthened shear to total $\Delta P_{max}^{95,t+s}$ decreases from 2040 through to 2100 as it is outpaced by the TCW increase. Hence, TCW remains the primary driver of increased MCS

extreme rainfall for all future time periods considering average driver changes across the Sahel.

4.1. Spatial variability of reconstructed extreme rainfall and comparison to modelled extremes

So far, presented results did not consider sub-regional driver variability. Across the Sahel domain, TCW changes show marked spatial variability linked to a pronounced zonal asymmetry in projected moisture changes as well as to generally strong meridional gradients in this wet-dry transition region (supplementary figures S2c, S3, S4). Strongest wind shear changes tend to follow zonal bands for CP4 and CMIP, for which most models suggest a peak in the eastern Sahel (supplementary figures S2d, S5, S6).

Assuming our domain-wide scaling factors remain valid locally, we calculate a pixel-based $\Delta P_{\max^{95},t+s}$ for the 2080 period in figures 4(a) and (b), showing the CMIP ensembles' 90th and 10th percentile, respectively. In line with model agreements on peaks of TCW and shear change in the eastern Sahel, the reconstructed $\Delta P_{\max^{95},t+s}$ shows highest values over Niger and northern Nigeria. Shear contributions to $\Delta P_{\max^{95},t+s} \geq 8\%$ up to a maximum of 17% (hatching) cover most of the northern Sahel for both extreme ends of the CMIP range, commensurate with large CMIP uncertainties in modelling changes in southern Saharan lower tropospheric warming (Rowell *et al* 2021).

Finally, we compare relative changes in reconstructed $\Delta P_{\max^{95},t+s}$ with modelled rainfall changes in CP4 and CMIP (figure 4(c)). The scaling is compared for the Sahel domain and boxes centred on the cities of Bamako (1), Timbuktu (2), and Niamey (3) (figure 4(a)), corresponding to regions along the previously discussed zonal gradient of TCW change projected by many CMIP models. For CP4, this step provides an indication of the skill of the simple linear driver-scaling presented here to reproduce regional intensities of modelled MCS rainfall. Figure 4(c) illustrates that for all regions except Bamako, the CP4-modelled $\Delta P_{\max^{95}}$ (black cross) lies within the uncertainty range of $\Delta P_{\max^{95},t+s}$ reconstructed from JAS CP4 driver changes (green cross and shading). The range reflects the uncertainty associated with the TCW and shear scaling factors and reaches a maximum of $\pm 7.7\%$ (Niamey). This good correspondence in spite of CP4's weak shear response may be linked to the scaling not considering additional rainfall intensification factors like instability, suggesting that our results may still be a conservative estimate.

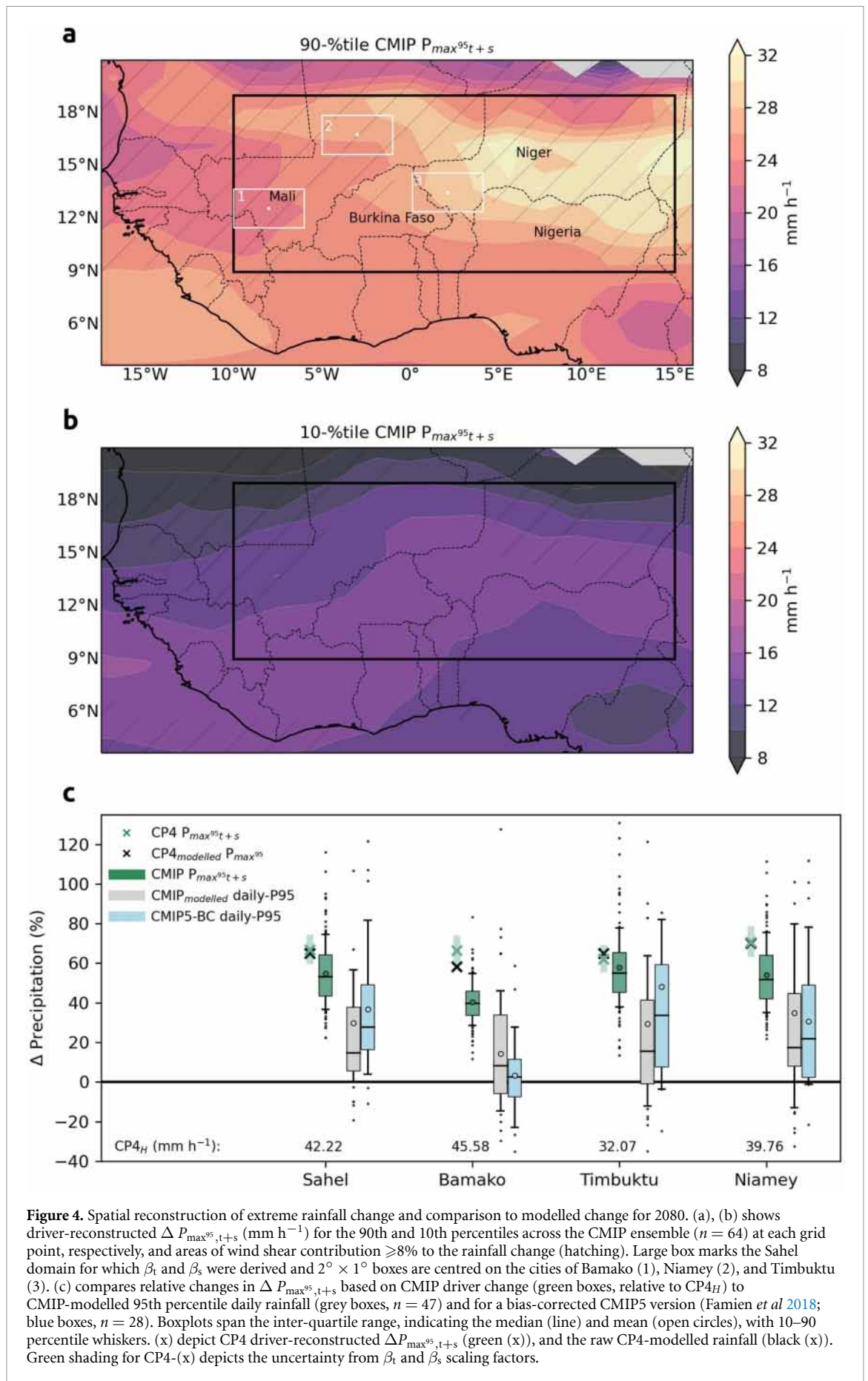
The CMIP5/6-based $\Delta P_{\max^{95},t+s}$ (green box) is shown in comparison to the modelled change in 95th percentile daily rainfall (for wet days ≥ 0.1 mm) of a range of raw CMIP5/6 models (grey box) as well as to a bias-corrected version of CMIP5 (blue box). We consider the latter to be the best available dataset regarding CMIP5-projected rainfall changes in West Africa (Famien *et al* 2018). Across evaluated regions,

the ensemble mean change in reconstructed extreme rainfall lies between +40% and 58% (+20%–31% for the 2040 period), which is markedly higher than for any ensemble-mean modelled CMIP rainfall in the same region. Furthermore, $\Delta P_{\max^{95},t+s}$ shows a clear signal of intensification across the entire CMIP uncertainty range, linked to exclusively positive driver changes. Modelled daily extremes on the other hand include negative changes within the 10–90th percentile CMIP range for all regions, with region-dependent ensemble means between 14% and 35% for raw CMIP and 3%–48% for bias-corrected CMIP5. While we acknowledge that the change in $\Delta P_{\max^{95},t+s}$, which is based on sub-daily extremes, may behave differently from CMIP daily rainfall metrics, it allows us to compare the reconstructed results to a more commonly-used and directly-inferred extreme rainfall metric. In addition, 3 out of 4 currently available CMIP6 models that provide sub-daily rainfall did not show a stronger signal for 3-hourly compared to daily extremes (supplementary figure S7), suggesting there is no systematic intensification at sub-daily scale that applies to all CMIP models.

5. Discussion and conclusions

In this study, our aim was to fuse a CP model projection, which provides us with only one possible future of how precipitation extremes from West African MCSs might change, with a CMIP-based time-continuous uncertainty range. For that, we adopted a simple linear scaling based on only TCW and shear, which we show allows to reconstruct CP4-modelled rainfall intensities. The presented scaling approach follows the assumption that CMIP changes in atmospheric drivers of MCSs are plausible, while the CP model in combination with observations provides a more realistic response of extreme MCS rainfall to those drivers. We thus draw on the strengths of respective datasets.

We find reconstructed changes in extreme rainfall to be exclusively positive across CMIP models, dominated by the strong projected increases in TCW with an ensemble 10–90 percentile range of +37%–75% (+55% mean) for 2070–2100 (+18%–30% with +26% mean for 2030–2060) under RCP8.5 across our Sahel domain. Shear contributions to these figures reach at least 8% for most of the northern Sahel, although we note that this result is based on MCS sensitivities to shear in the afternoon. The shear contribution may be higher for nocturnal MCSs, when the importance of shear for MCS maintenance increases in the absence of daytime heating (e.g. Vizy and Cook 2018). The strictly positive changes are in contrast to CMIP-modelled changes in daily extremes, which we find to be less conclusive with a 10–90 percentile range of +0–60% (+30% mean) for raw CMIP5/6 rainfall and +4%–88% (+37%



mean) using a bias-corrected CMIP5 dataset with some models again exhibiting negative changes.

The limited previous analyses of extreme rainfall projections over West Africa to date focus on selections of RCP8.5 downscaled CMIP models and have found either little change in extreme precipitation trends compared to driving CMIP models with no agreement in sign (Diallo *et al* 2016) or end-of-century ensemble-mean increases that stay below 40% (Sylla *et al* 2015, Todzo *et al* 2020). This suggests, CMIP and even medium-resolution downscaling approaches may consistently underestimate extreme rainfall change, potentially in ways related to model resolution, convection schemes and projected driver changes. This conclusion is further supported by previous CP4 studies (Kendon *et al* 2019, Finney *et al* 2020, Jackson *et al* 2020).

While the driver-reconstructed change in extreme rainfall presented here exhibits an apparently smaller uncertainty range than that of the CMIP models, many assumptions and simplifications are incorporated in the reconstruction that are not explicitly reflected. For example, we assume that the driver changes MCSs feel locally on an hourly basis are proportional to the climate change in the July–September domain mean as represented in the CMIP driver data. We also necessarily assume that rainfall scaling with wind shear is stationary across climates since the CP model fails to capture the observed shear sensitivity, highlighting a key problem of this CP simulation—although related errors would be minor given the indicated secondary role of wind shear for future extreme rain intensification. Furthermore, various scaling problems are simplified by the fact that all changes in the considered drivers are positive and force extreme rain in the same direction with climate change, avoiding drivers cancelling each other, which would considerably increase the significance of scaling errors. We also use the historical CP4 rainfall distribution as a present-day reference to translate the reconstructed absolute rainfall changes into relative changes, even though certain CMIP future driver changes may be unlikely given the CP4 historical starting point. Nevertheless, for simplicity, we assume all CMIP driver changes to be equally plausible to occur in CP4.

This leaves us with a novel methodology that combines CP with CMIP simulations and observations to translate future atmospheric changes into extreme rainfall change. The reconstructed extreme rainfall illustrates that, given the background conditions for MCS formation in a region, associated rainfall extremes will increase in line with and beyond the regional increase in TCW if relative humidity remains approximately constant. This relationship, diagnosed from CP simulations, makes TCW change a useful indicator for the behaviour of the extreme tail of the rainfall distribution. In this way, an evaluation of convection-permitting rainfall projections based

on atmospheric drivers helps to communicate to users more defensible hydro-climatological information for West Africa, using our best scientific knowledge and understanding of the likely future changes in MCSs. The logical framing of this approach also lends itself to the construction of climate-change narratives (e.g. Dessai *et al* 2018, Burgin *et al* 2020), which have been found to be very useful in risk communication.

Data availability statement

The data that support the findings of this study are available upon reasonable request from the authors.

Acknowledgments

The research leading to these results received funding from the U.K.'s Natural Environment Research Council/Department for International Development (NERC/DFID) Future Climate for Africa (FCFA) program, under the AMMA-2050 (Grant Numbers NE/M020126/1, NE/M019977/1, NE/M019969/1, NE/M019950/1, NE/M019934/1, NE/M020428/2, NE/M020428/1) and Improving Model Processes for African Climate (IMPALA) projects (NE/MO17176/1, NE/M017230/1). Marsham also acknowledges funding from the HyCRISTAL project (NE/M02038X/1). We thank Rachel Stratton and Simon Vosper (Met Office), who ran the CP4 simulations within IMPALA and made the data available. Instructions for access to the CP4 dataset can be found in the User Guide via <https://doi.org/10.5281/zenodo.4316466> and are publicly available from the Centre for Environmental Data Analysis (CEDA) archive (<http://archive.ceda.ac.uk/>). The bias-corrected CMIP5 dataset can be obtained by contacting A D: moise.famien@locean.ipsl.fr. MSG data are available from the EUMETSAT archive <https://navigator.eumetsat.int/product/EO:EUM:DAT:MSG:HRSEVIRI>, ECMWF hourly ERA5 reanalysis data are available from the Copernicus Data Store (<https://doi.org/10.24381/cds.bd0915c6>) and data from the Global Precipitation Measurement mission are available from <https://doi.org/10.5067/GPM/IMERG/3B-HH/06>. We also acknowledge the World Climate Research Programme, which, through its Working Group on Coupled Modelling, coordinated and promoted CMIP. We thank the climate modeling groups for producing and making available their model output, the Earth System Grid Federation (ESGF) for archiving the data and providing access, and the multiple funding agencies who support CMIP5 (<https://esgf-node.llnl.gov/projects/cmip5/>), CMIP6 and ESGF, and we thank the involved climate modeling groups for producing and making available their model output. Special thanks go to the developers

of the Pangeo CMIP6 data access and cloud processing (https://pangeo-data.github.io/pangeo-cmip6-cloud/accessing_data.html), which worked like a charm, and to the providers of the python packages matplotlib/cartopy, xarray, salem, scipy, metpy, pandas, and their dependencies.

Author contributions


C K, L J, D P, J M, C T, D R and F G conceptualised the study, with input from T V and A D. All authors contributed to and discussed the methodological design, and analyses were conducted by C K and L J, with input from A F. C K and D P led the writing of the manuscript, with contributions from all authors.

ORCID iDs

Cornelia Klein  <https://orcid.org/0000-0001-6686-0458>

Lawrence S Jackson  <https://orcid.org/0000-0001-8143-2777>

Douglas J Parker  <https://orcid.org/0000-0003-2335-8198>

Christopher M Taylor  <https://orcid.org/0000-0002-0120-3198>

Adjoua Moïse Famien  <https://orcid.org/0000-0002-4551-7033>

Arona Diedhiou  <https://orcid.org/0000-0003-3841-1027>

References

- Alfaro D A 2017 Low-tropospheric shear in the structure of squall lines: impacts on latent heating under layer-lifting ascent *J. Atmos. Sci.* **74** 229–48
- Allen M R and Ingram W J 2002 Constraints on future changes in climate and the hydrologic cycle *Nature* **419** 228–32
- Arnaud Y, Desbois M and Maizi J 1992 Automatic tracking and characterization of African convective systems on Meteosat pictures *J. Appl. Meteorol.* **31** 443–53
- Berthou S, Kendon E J, Rowell D P, Roberts M J, Tucker S and Stratton R A 2019 Larger future intensification of rainfall in the West African Sahel in a convection-permitting model *Geophys. Res. Lett.* **46** 13299–307
- Berthou S, Rowell D P, Kendon E J, Roberts M J, Stratton R A, Crook J A and Wilcox C 2019 Improved climatological precipitation characteristics over West Africa at convection-permitting scales *Clim. Dyn.* **53** 1991–2011
- Bickle M E, Marsham J H, Ross A N, Rowell D P, Parker D J and Taylor C M 2021 Understanding mechanisms for trends in Sahelian squall lines: roles of thermodynamics and shear *Q. J. R. Meteorol. Soc.* **147** 983–1006
- Brunner M I, Slater L, Tallaksen L M and Clark M 2021 Challenges in modeling and predicting floods and droughts: a review *WIREs Water* **8** e1520
- Burgin L, Rowell D P and Marsham J H 2020 Possible futures for East Africa under a changing climate: Technical appendix for HyCRISTAL's Climate Risk Narratives (<https://doi.org/10.5281/zenodo.3257287>)
- CDS 2021 Copernicus Climate Data Store: ERA, Fifth generation of ECMWF atmospheric reanalyses of the global climate (available at: <https://cds.climate.copernicus.eu/cdsapp#/dataset/reanalysis-era5-pressure-levels?tab=overview>) (Accessed 14 January 2020)
- Coppola E et al 2020 A first-of-its-kind multi-model convection permitting ensemble for investigating convective phenomena over Europe and the Mediterranean *Clim. Dyn.* **55** 1–2
- Crook J, Klein C, Folwell S, Taylor C M, Parker D J, Stratton R and Stein T 2019 Assessment of the Representation of West African Storm Lifecycles in Convection-Permitting Simulations *Earth Space Sci.* **6** 818–35
- Dessai S, Bhawe A, Birch C, Conway D, Garcia-Carreras L, Gosling J P, Neha M and Stainforth D 2018 Building narratives to characterise uncertainty in regional climate change through expert elicitation *Environ. Res. Lett.* **13** 074005
- Diallo I, Giorgi F, Deme A, Tall M, Mariotti L and Gaye A T 2016 Projected changes of summer monsoon extremes and hydroclimatic regimes over West Africa for the twenty-first century *Clim. Dyn.* **47** 3931–54
- Engel T, Fink A H, Knippertz P, Pante G and Bliedernicht J 2017 Extreme precipitation in the West African cities of Dakar and Ouagadougou: atmospheric dynamics and implications for flood risk assessments *J. Hydrometeorol.* **18** 2937–57
- EUMETSAT 2021 High Rate SEVIRI Level 1.5 Image Data - MSG - 0 degree (available at: <https://navigator.eumetsat.int/product/EO:EUM:DAT:MSG:HRSEVIRI>) (Accessed 25 August 2021)
- Eyring V, Bony S, Meehl G A, Senior C A, Stevens B, Stouffer R J and Taylor K E 2016 Overview of the coupled model intercomparison project phase 6 (CMIP6) experimental design and organization *Geosci. Model Dev.* **9** 1937–58
- Famien A M, Janicot S, Delfin Ochoa A, Vrac M, Defrance D, Sultan B and Noël T 2018 A bias-corrected CMIP5 dataset for Africa using the CDF-t method—a contribution to agricultural impact studies *Earth Syst. Dyn.* **9** 313–38
- Field P R et al 2017 Exploring the convective grey zone with regional simulations of a cold air outbreak *Q. J. R. Meteorol. Soc.* **143** 2537–55
- Finney D L et al 2020 Effects of explicit convection on future projections of mesoscale circulations, rainfall and rainfall extremes over eastern Africa *J. Clim.* **33** 2701–18
- Fitzpatrick R G, Parker D J, Marsham J H, Rowell D P, Guichard F M, Taylor C M and Tucker S 2020 What drives the intensification of mesoscale convective systems over the West African Sahel under climate change? *J. Clim.* **33** 3151–72
- Fosser G, Kendon E J, Stephenson D and Tucker S 2020 Convection-permitting models offer promise of more certain extreme rainfall projections *Geophys. Res. Lett.* **47** 0–2
- François B, Schlef K, Wi S and Brown C 2019 Design considerations for riverine floods in a changing climate—a review *J. Hydrol.* **574** 557–73
- Hersbach H et al 2020 The ERA5 global reanalysis The ERA5 global reanalysis *Q. J. R. Meteorol. Soc.* **146** 1999–2049
- Huffman G, Stocker E, Bolvin D, Nelkin E and Tan J 2019 GPM IMERG Final Precipitation L3 Half Hourly 0.1 degree × 0.1 degree V06, Greenbelt, MD, Goddard Earth Sciences Data and Information Services Center (GES DISC) vol 01 (available at: https://disc.gsfc.nasa.gov/datasets/GPM_3IMERGHH_06/summary) (Accessed 25 August 2021)
- IPCC 2021 *Climate Change 2021: The Physical Science Basis. Contribution of Working Group I to the Sixth Assessment Report of the Intergovernmental Panel on Climate Change* ed V Masson-Delmotte et al (Cambridge University Press) (<https://www.ipcc.ch/report/sixth-assessment-report-working-group-i/>)
- Jackson L S, Finney D L, Kendon E J, Marsham J H, Parker D J, Stratton R A, Tomassini L and Tucker S 2020 The effect of explicit convection on couplings between rainfall, humidity and ascent over Africa under climate change *J. Clim.* **33** 8315–37
- Jones C D et al 2011 The HadGEM2-ES implementation of CMIP5 centennial simulations *Geosci. Model Dev.* **4** 543–70

- Kendon E J, Ban N, Roberts N M, Fowler H J, Roberts M J, Chan S C, Evans J P, Fosser G and Wilkinson J M 2017 Do convection-permitting regional climate models improve projections of future precipitation change? *Bull. Am. Meteorol. Soc.* **98** 79–93
- Kendon E J, Stratton R A, Tucker S, Marsham J H, Berthou S, Rowell D P and Senior C A 2019 Enhanced future changes in wet and dry extremes over Africa at convection-permitting scale *Nat. Commun.* **10** 1794
- Klein C, Nkrumah F, Taylor C M and Adefisan E A 2021 Seasonality and trends of drivers of mesoscale convective systems in Southern West Africa *J. Clim.* **34** 71–87
- Lafore J P et al 2011 Progress in understanding of weather systems in West Africa *Atmos. Sci. Lett.* **12** 7–12
- Laing A G, Fritsch J M and Negri A J 1999 Contribution of mesoscale convective complexes to rainfall in Sahelian Africa: estimates from geostationary infrared and passive microwave data *J. Appl. Meteorol.* **38** 957–64
- Lavin-Gullon A, Feijoo M, Solman S, Fernandez J, da Rocha R P and Bettolli M L 2021 Synoptic forcing associated with extreme precipitation events over Southeastern South America as depicted by a CORDEX FPS set of convection-permitting RCMs *Clim. Dyn.* **56** 3187–203
- Lenderink G, de Vries H, Fowler H J, Barbero R, van Ulft B and van Meijgaard E 2021 Scaling and responses of extreme hourly precipitation in three climate experiments with a convection-permitting model *Phil. Trans. R. Soc. A* **379** 20190544
- Lobell D B and Gourdji S M 2012 The influence of climate change on global crop productivity *Plant Physiol.* **160** 1686–97
- Maranan M, Fink A H and Knippertz P 2018 Rainfall types over southern West Africa: objective identification, climatology and synoptic environment *Q. J. R. Meteorol. Soc.* **144** 1628–48
- Mathon V and Laurent H 2001 Life cycle of Sahelian mesoscale convective cloud systems *Q. J. R. Meteorol. Soc.* **127** 377–406
- Mathon V, Laurent H and Lebel T 2002 Mesoscale convective system rainfall in the Sahel *J. Appl. Meteorol.* **41** 1081–92
- Mohr K I and Thorncroft C D 2006 Intense convective systems in West Africa and their relationship to the African easterly jet *Q. J. R. Meteorol. Soc.* **132** 163–76
- Moseley C, Hohenegger C, Berg P and Haerter J O 2016 Intensification of convective extremes driven by cloud-cloud interaction *Nat. Geosci.* **9** 748–52
- Mulholland J P, Peters J M and Morrison H 2021 How does vertical wind shear influence entrainment in squall lines? *J. Atmos. Sci.* **78** 1931–46
- Nicholson S E 2018 Climate of the Sahel and West Africa Oxford Research Encyclopedia of Climate Science (Oxford: Oxford University Press) (<https://doi.org/10.1093/acrefore/9780190228620.013.510>)
- O’Gorman P A and Schneider T 2009 The physical basis for increases in precipitation extremes in simulations of 21st-century climate change *Proc. Natl Acad. Sci. USA* **106** 14773–7
- Prein A F et al 2015 A review on regional convection-permitting climate modeling: demonstrations, prospects and challenges *Rev. Geophys.* **53** 323–61
- Prein A F, Liu C, Ikeda K, Trier S B, Rasmussen R M, Holland G J and Clark M P 2017 Increased rainfall volume from future convective storms in the US *Nat. Clim. Change* **7** 880–4
- Reynolds R W, Smith T M, Liu C, Chelton D B, Casey K S and Schlax M G 2007 Daily high-resolution-blended analyses for sea surface temperature *J. Clim.* **20** 5473–96
- Roderick T P, Wasko C and Sharma A 2019 Atmospheric moisture measurements explain increases in tropical rainfall extremes *Geophys. Res. Lett.* **46** 1375–82
- Rowell D P, Fitzpatrick R G, Jackson L S and Redmond G 2021 Understanding intermodel variability in future projections of a Sahelian storm proxy and southern saharan warming *J. Clim.* **34** 509–25
- Sane Y et al 2018 Intensity-duration-frequency (IDF) rainfall curves in Senegal *Nat. Hazards Earth Syst. Sci.* **18** 1849–66
- Schmetz J, Pili P, Tjemkes S, Just D, Kerkmann J, Rota S and Ratier A 2002 An introduction to meteosat second generation (MSG) *Bull. Am. Meteorol. Soc.* **83** 977–92
- Senior C A et al 2021 Convection permitting regional climate change simulations for understanding future climate and informing decision making in Africa *Bull. Am. Meteorol. Soc.* **102** E1206–23
- Sharma A, Hettiarachchi S and Wasko C 2021 Estimating design hydrologic extremes in a warming climate: alternatives, uncertainties and the way forward *Phil. Trans. R. Soc. A* **379** 20190623
- Stephens G L, L’Ecuyer T, Forbes R, Gettleman A, Golaz J C, Bodas-Salcedo A, Suzuki K, Gabriel P and Haynes J 2010 Dreary state of precipitation in global models Dreary state of precipitation in global models *J. Geophys. Res. Atmos.* **115** 1–14
- Stratton R A et al 2018 A Pan-African convection-permitting regional climate simulation with the met office unified model: CP4-Africa *J. Clim.* **31** 3485–508
- Sylla M B, Giorgi F, Pal J S, Gibba P, Kebe I and Nikiema M 2015 Projected changes in the annual cycle of high-intensity precipitation events over West Africa for the late twenty-first century *J. Clim.* **28** 6475–88
- Taylor K E, Stouffer R J and Meehl G A 2012 An overview of CMIP5 and the experiment design *Bull. Am. Meteorol. Soc.* **93** 485–98
- Todzo S, Bichet A and Diedhiou A 2020 Intensification of the hydrological cycle expected in West Africa over the 21st century *Earth Syst. Dyn.* **11** 319–28
- Trenberth K E, Dai A, Rasmussen R M and Parsons D B 2003 The changing character of precipitation *Bull. Am. Meteorol. Soc.* **84** 1205–17
- Vischel T and Lebel T 2007 Assessing the water balance in the Sahel: Impact of small scale rainfall variability on runoff. Part 2: idealized modeling of runoff sensitivity *J. Hydrol.* **333** 340–55
- Vizy E K and Cook K H 2018 Mesoscale convective systems and nocturnal rainfall over the West African Sahel: role of the Inter-tropical front *Clim. Dyn.* **50** 587–614
- Zhou X, Yang K, Ouyang L, Wang Y, Jiang Y, Li X, Chen D and Prein A 2021 Added value of kilometer-scale modeling over the third pole region: a CORDEX-CPTP pilot study *Clim. Dyn.* **57** 1673–87